

Supplementary Material for

**Sub-Angstrom Edge Relaxations Probed by Electron
Microscopy in Hexagonal Boron Nitride (h-BN)**

Nasim Alem^{1,2,3}, Quentin M. Ramasse^{4,*}, Che R. Seabourne⁵, Oleg V. Yazyev^{1,3,6},
Kris Erickson^{1,3}, Michael C. Sarahan⁴, Christian Kisielowski⁷, Andrew J. Scott⁵,
Steven G. Louie^{1,3}, and A. Zettl^{1,3}

*To whom correspondence should be addressed

¹Department of Physics, University of California Berkeley, California 94720, USA

²Center of Integrated Nanomechanical Systems, University of California Berkeley,
94720, USA

³Materials Sciences Division, Lawrence Berkeley National Laboratory, Berkeley,
California 94720, USA

⁴SuperSTEM Laboratory, STFC Daresbury, Keckwick Lane, Daresbury WA4 4AD, U.K.

⁵Institute for Materials Research, SPEME, University of Leeds, Leeds LS2 9JT, U.K.

⁶Institute of Theoretical Physics, Ecole Polytechnique Fédérale de Lausanne (EPFL), CH-
1015 Lausanne, Switzerland

⁷National Center for Electron Microscopy and Joint Center for Artificial Photosynthesis,
Lawrence Berkeley National Laboratory, Berkeley, California 94720, USA

I. Instrumentation

All experimental work was carried out on a Nion UltraSTEM 100 dedicated scanning transmission electron microscope [1], equipped with a cold field emission gun and operated at 60 keV primary beam energy in order to minimize knock-on damage to the sample. The instrument column has a metal seal design throughout, which allows for clean vacuum conditions at the sample (lower than 5×10^{-9} Torr) for contamination-free observation. The probe forming optics were aligned to deliver a 29 mrad convergence semi-angle with 50 pA of beam current. In these conditions, and after correction of electron optical aberrations up to fifth order, the estimated probe size is 1.1 Å.

Two different detector angular ranges can be used for annular dark field (ADF) imaging: the inner and outer radii for the high angle annular dark field (HAADF) detector were 85 to 195 mrad and for the medium angle annular dark field (MAADF) detector were 55 to 195 mrad. All images were recorded in MAADF mode except where explicitly stated. In order to reduce the noise levels and to improve the accuracy of the image analysis, a probe deconvolution algorithm based on maximum entropy methods was applied to the raw ADF images. All images in the main manuscript were processed using this algorithm, which also has the advantage of removing the contribution of the tails of the focused electron probe to the neighboring atom intensities, which is essential for quantitative contrast analysis [2].

Although in the operating conditions the beam energy spread is approximately 0.35 eV (as estimated using the full width at half-maximum of the zero-loss beam), the electron energy loss spectra were acquired using an energy dispersion of 0.30 eV per channel and the spectrum resolution is therefore limited by the camera point spread function.

II. Sample preparation:

Hexagonal boron nitride powder was used for this investigation. The powder used in this experiment was purchased from Momentive Performance Materials. The powder was mechanically exfoliated and transferred to the TEM grid as previously reported [3, 4]. Using optical microscopy, thin BN flakes are transferred to the TEM grid.

A Quantifoil gold TEM grid with a perforated carbon film with hole size of 1.2 μm is placed on top of the BN flake and a drop of isopropanol alcohol is placed on the grid and left to dry. Then a drop of polyimide is placed on the TEM grid and the sample is heated at 110°C for 10 min. After heating, the polyimide is peeled off in one piece, enclosing the TEM grid and the now-adhered BN flake. The sample is placed in a methylpyrrolidone bath for a few hours at 60°C to dissolve the polyimide. The TEM grid is then transferred to isopropanol solution for a few minutes and dried. The samples were screened in conventional bright field TEM mode in a JEOL 2010 electron microscope to locate the thinnest flakes prior to observation in the STEM. Due to its polar nature, h-BN forms preferentially combinations of even numbers of layer. It was thus possible to locate in the thinnest flakes many large areas consisting predominantly of bilayer h-BN. The step-wise contrast changes next to holes in the sample, and the very characteristic contrast of single-layer patches of h-BN [2] confirmed straightforwardly the identification of the sheet as bilayer.

III. Image and EELS spectra recording condition

Although the experiments were carried out in so-called gentle STEM conditions [5] (low primary beam energy and clean vacuum conditions along), the beam energy was still sufficient to impart visible knock-on damage to the sample after repeated scanning, resulting in the formation of vacancies, terraces, step edges, and holes (Fig. S1).

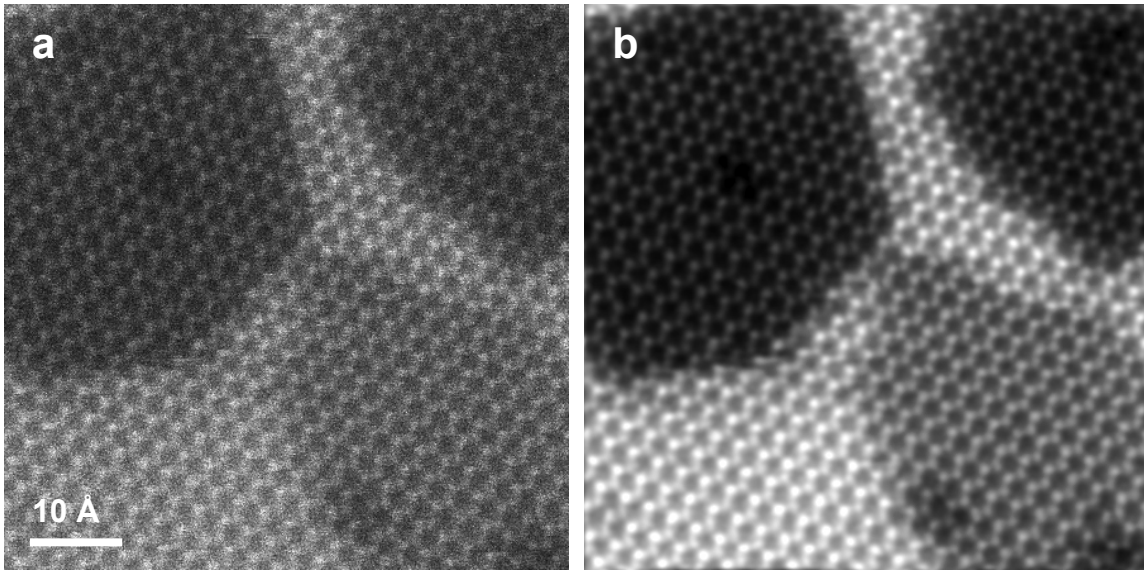


Fig. S1. (a) Raw and (b) denoised Annular Dark Field (ADF) image of few layer h-BN showing formation of vacancies, terraces and zigzag step edges due to knock-on beam damage at 60 keV.

The following raw image in Fig. S2 shows an ADF image of the h-BN film (a processed version of which is shown as Fig. 1 of the main text) after the atoms are sputtered away and a hole is formed within the membrane.

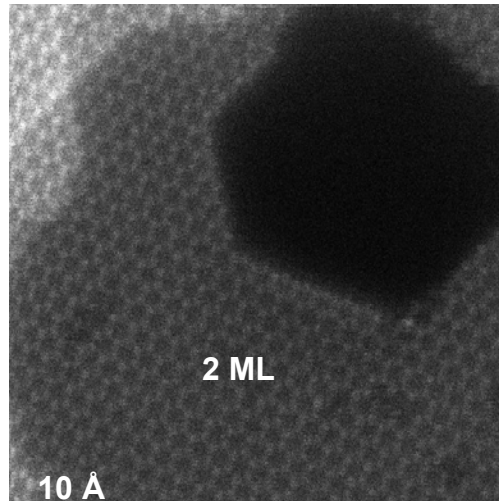


Fig. S2. The raw ADF image of a bilayer h-BN showing formation of a hole and zigzag edges as a result of the knock-on beam damage on the sample.

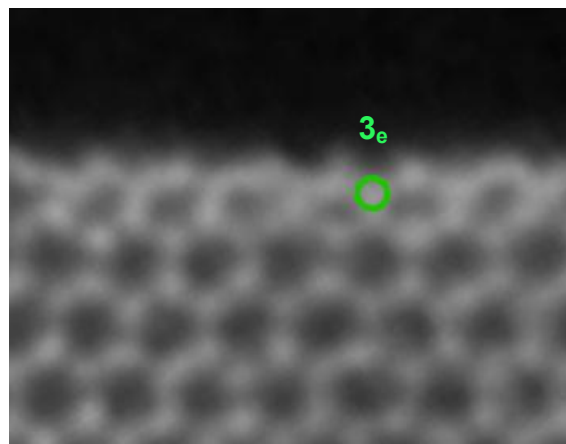


Fig. S3. HAADF image of a bilayer h-BN. The green marker shows the actual location of the beam that resulted in the EELS spectrum 3_e presented in the paper in Fig. 3.

As indicated in Fig. 3 of the paper, three types of atomic positions were probed by EELS at the edge of the BN edge membrane, labeled 1_e, 2_e and 3_e. Although the label 3_e in Fig. 3 of the paper shows an equivalent column position with respect to the edge, the EEL spectrum was acquired by positioning the beam using a different 'survey' image, for a slightly different area of the sample. The green marker on Fig. S3 shows the actual

location of the beam and the actual image (an HAADF image of a bilayer h-BN edge) which resulted in the spectrum shown in the paper.

Fig. S4 shows formation of a hole in a monolayer of h-BN and the chemical identification of the unit cell from the ADF image within the monolayer. This identification confirms formation of nitrogen terminating zigzag edges and vacancy formation as a result of the ejection of boron atoms from the lattice at 60 keV [2].

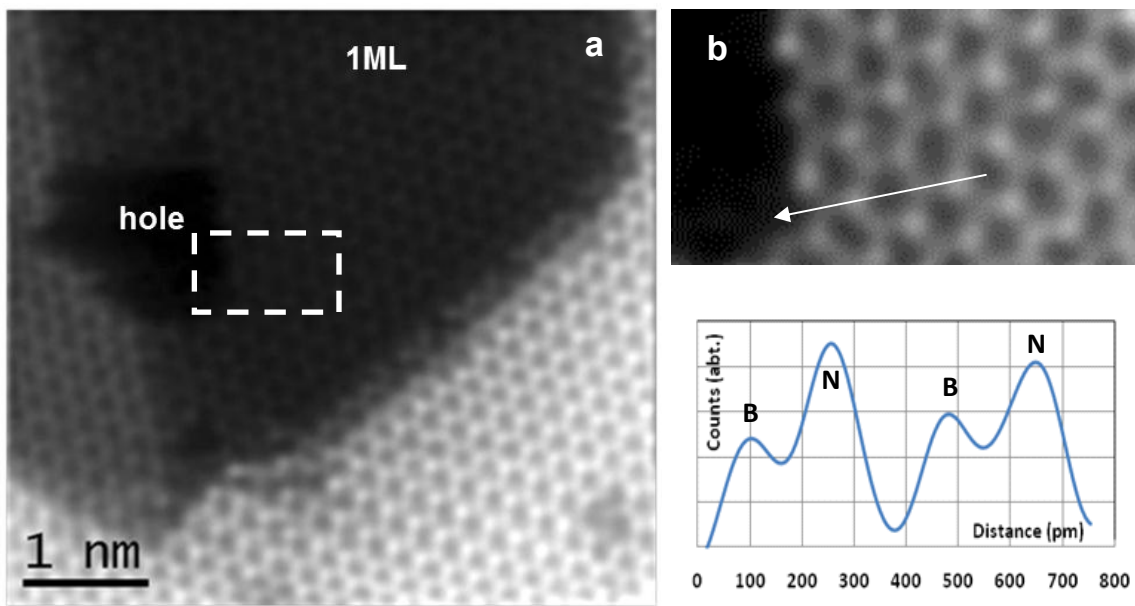
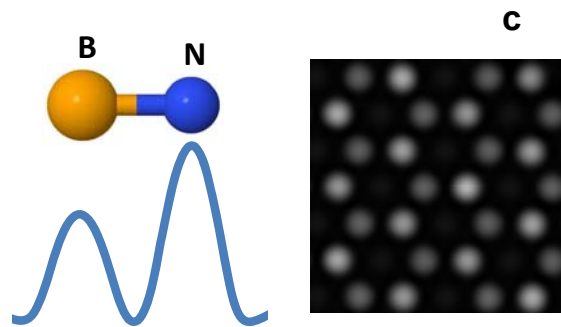


Fig. S4. ADF image of the film showing the formation of a hole in a monolayer of h-BN (a). A closer look at the signal in the line profile shows a higher atomic Z contrast to the right side of the unit cell



(b). Annular dark field STEM image simulations similarly show a higher Z contrast for the nitrogen atom on the right side of the unit cell (c).

IV. STEM Image Simulations

Annular dark field images were simulated using the MacTempas software in this study. A semi-angle of 29 mrad was considered for the probe-forming aperture. The inner and outer angles for the annular-dark-field detector were adjusted to the experimental values of 50 to 190 mrad, which corresponds in reciprocal space to reflections up to a “g” vector of 8 ($1/\text{\AA}$).

A frozen phonon model with 10 different configurations was incorporated in the simulations. At 60 keV primary beam energy and in a well-tuned C_3/C_5 -corrected instrument, the probe size is typically limited by chromatic aberration (in the experimental conditions used here, the chromatic aberration coefficient is 1.3 mm and the energy spread of 0.35 eV) [6]: the beam conditions in the STEM image simulations resulted in a probe size of about 1 \AA , which is similar to probe size in the experiment.

V. First-Principles Calculations

V. A. Structural Distortions

First-principles calculations of bilayer h-BN edges (AA' stacking) were performed using bilayer nanoribbon models of 2 nm width. The calculations were performed within the local density approximation using the pwscf plane-wave pseudopotential code of the Quantum-ESPRESSO distribution [7]. Ultrasoft pseudo-potentials were used to describe core-valence interactions [8]. The valence wave functions and the electron density were described by plane-wave basis sets with kinetic energy cutoffs of 30 Ry and 300 Ry, respectively. Fig. S5 presents the h-BN model considered for these calculations before and after relaxations.

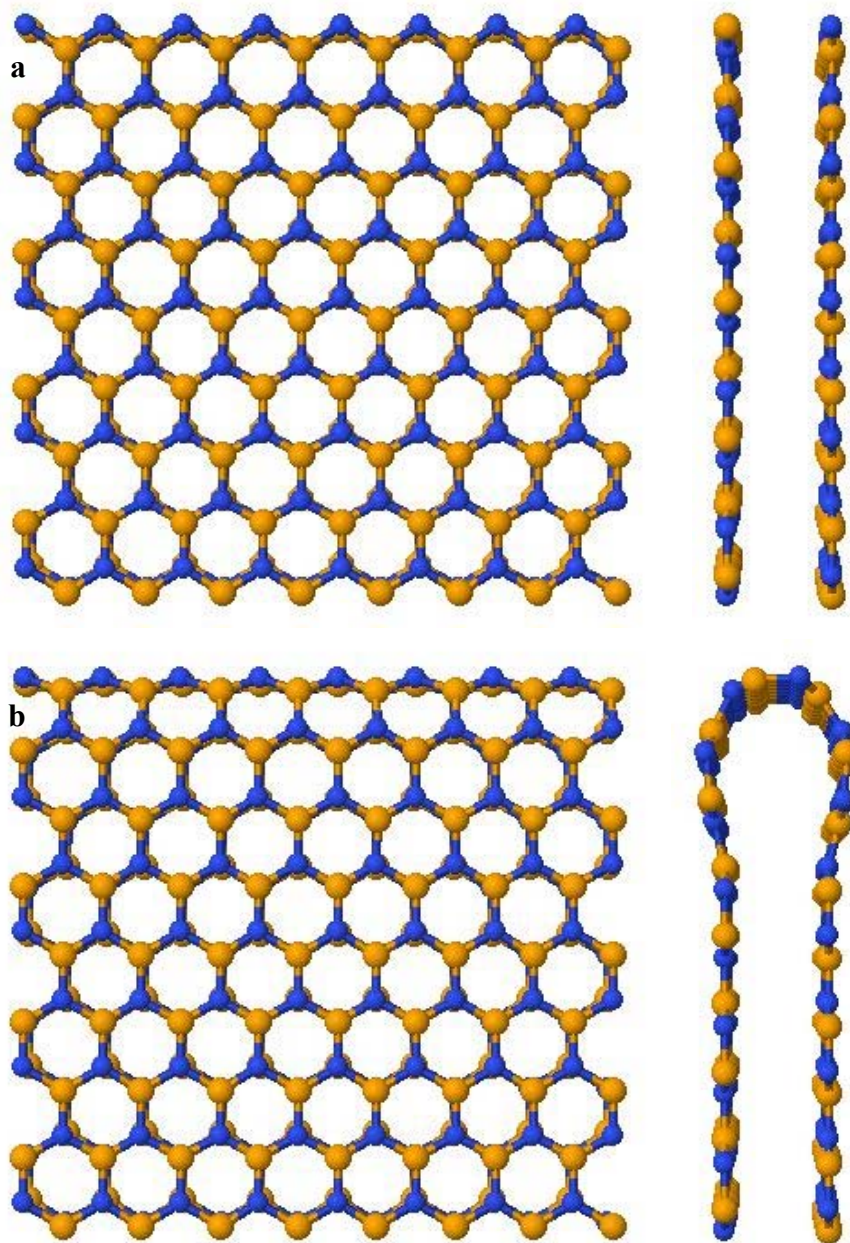


Fig. S5. Cross-sectional and plan view of the structural model for the bilayer h-BN used in the first-principles calculations. The structural model in (a) shows the bilayer h-BN before any relaxations occur at the edge of the bilayer h-BN. The schematic in (b) shows this structure after the top edge of the bilayer is allowed to relax. Boron is orange, and nitrogen is blue.

V.B. EELS Edge Simulations

All EELS calculations carried out in this work were performed using the CASTEP code [9]. CASTEP is a pseudopotential code, using a plane wave basis set, within the Kohn-Sham formalism [10, 11]. For all the reported calculations, the generalized gradient approximation (GGA) was used [12]. Recent developments have allowed electron energy-loss spectroscopy (EELS) to be simulated using the CASTEP code. The physical background behind the additions is detailed extensively in the literature [13, 14]. The work is based on the projector augmented wave (PAW) approach [15, 16]. In this methodology, the first consideration is the type of core-loss edge being considered. For a K edge (the only type of edge modeled in this work), provided that the dipole selection rule applies, the p orbital partial density of states (DOS) must be found. Subsequently, transition matrix elements between the initial and final states must be determined. These effectively express the ‘probability’ for a given transition between an initial and final state. When using a DFT code to perform EELS simulations, the key DFT code parameters to consider are the basis set size (i.e. the choice of kinetic energy cut-off value), and the quality of sampling in reciprocal space (i.e. the k -point mesh density). These parameters were converged specifically against the predicted EELS result, following a systematic approach as previously outlined by some of the authors of this paper [17, 18]. In this work, the convergence system used was hexagonal boron nitride ($a = b = 2.50 \text{ \AA}$, $c = 6.66 \text{ \AA}$, $\alpha = \beta = 90^\circ$, $\gamma = 120^\circ$).

The kinetic energy cut-off was increased in steps of 100 eV from a starting value of 300 eV. In all cases a 0.30 eV Gaussian broadening was then applied (corresponding to the microscope native energy spread). Following each sequential change, a numerical

analysis was carried out to determine if convergence had been achieved. For each energy-axis point, the difference in the predicted intensity between for example, the data obtained using a 400 eV and then a 500 eV cut-off was found. That difference in value was then used to find a percentage change in intensity, with these then being averaged across a data range of -2 eV to 30 eV above the Fermi level (in intervals of ± 0.05 eV). When this value was less than 10% the parameter was considered to be converged. This therefore led to a value of 500 eV being used for the kinetic energy cut-off. In terms of the k -point sampling, the number of k -points was doubled in each dimension until the average percentage intensity change was again less than 10%. This meant that the k -point spacing in each dimension was 0.029 \AA^{-1} or better. For the pristine bilayer of boron nitride, a total c dimension of 25 \AA was sufficient (i.e. a vacuum spacing of $\sim 20 \text{ \AA}$ to separate the bilayers in the periodic repeating structure), with the two layers themselves being separated by 3.53 \AA . For the distorted structure, similar vacuum spacings were utilized wherever required. The predicted spectra have been aligned relative to each other as indicated in Figure 3. It would have been possible to argue for different alignments, but these would not have modified the conclusion that the modeling supports the relaxed rather than pristine model as outlined in that figure.

References:

- [1] O. L. Krivanek *et al.*, Ultramicroscopy **108**, 179 (2008).
- [2] O. L. Krivanek *et al.*, Nature **464**, 571 (2010).
- [3] N. Alem *et al.*, Phys Rev B **80**, 155425 (2009).
- [4] D. Pacile *et al.*, Appl Phys Lett **92**, 133107 (2008).
- [5] O. L. Krivanek *et al.*, Ultramicroscopy **110**, 935 (2010).
- [6] O. L. Krivanek *et al.*, *Atomic-resolution STEM at low primary energies* Springer, New York, 613 (2011).
- [7] P. Giannozzi *et al.*, J Phys-Condens Mat **21**, 395502 (2009).
- [8] D. Vanderbilt, Phys Rev B **41**, 7892 (1990).

- [9] S. J. Clark *et al.*, *Z Kristallogr* **220**, 567 (2005).
- [10] W. Kohn, and L. J. Sham, *Phys Rev* **140**, A1133 (1965).
- [11] M. C. Payne *et al.*, *Rev Mod Phys* **64**, 1045 (1992).
- [12] J. P. Perdew, K. Burke, and M. Ernzerhof, *Phys Rev Lett* **77**, 3865 (1996).
- [13] S. P. Gao *et al.*, *Phys Rev B* **77**, 115122 (2008).
- [14] V. Milman *et al.*, *J Mol Struct-Theochem* **954**, 22 (2010).
- [15] P. E. Blochl, *Phys Rev B* **50**, 17953 (1994).
- [16] C. J. Pickard, *Ab initio electron energy loss spectroscopy*, Ph.D. Thesis, University of Cambridge (1997).
- [17] C. R. Seabourne *et al.*, *Ultramicroscopy* **109**, 1374 (2009).
- [18] C. R. Seabourne *et al.*, *Ultramicroscopy* **110**, 1059 (2010).